Journal of Materials Research and Technology 43 (2026) 5750–5754

Contents lists available at ScienceDirect

Journal of Materials Research and Technology

journal homepage: www.elsevier.com/locate/jmrt

Influence of differences in wrought processes on mechanical properties of AZ31 magnesium alloy

Hiromasa Yoshizumi [a,*], Motohiro Yuasa [a,**], Hiroyuki Miyamoto [a], Hidetoshi Somekawa [b]

[a] Faculty of Science and Engineering, Doshisha University, 1-3 Miyakodani, Tatara, Kyotanabe, Kyoto, 610-0394, Japan

[b] Research Center for Structural Materials, National Institute for Materials Science, 1-2-1 Sengen, Tsukuba, Ibaraki, 305-0047, Japan

ARTICLE INFO

Keywords:
Magnesium alloy
Mechanical property
Finite element method
Work hardening
Basal texture

ABSTRACT

The influence of different wrought processes on the mechanical properties of AZ31 magnesium alloy was investigated in terms of the strain state induced during these processes using a combination of finite element method (FEM) analysis and tensile testing. A process with a large compressive strain develops an intensive basal texture, leading to high strength and poor ductility.

1. Introduction

Various wrought processes have been used to enhance the mechanical properties of magnesium (Mg) alloys through grain refinement [1–5]. Nevertheless, the influence of differences in the wrought process on the mechanical properties has not been clarified. The wrought processes are characterized quantitatively using the induced equivalent strain and strain state (strain components). A larger equivalent strain promotes dynamic recrystallization and refines grain size, resulting in improved hardness [6,7]. When different processes induce the same equivalent strain, the deformed microstructure and texture depend on the strain path [3,8,9]. Because the strain path varies with the strain components, the results of these studies indicate that the strain components affect the microstructure and texture evolution, apart from the equivalent strain. Several studies have investigated the influence of the strain state on the microstructure and texture evolution using the finite element method (FEM) [9–13]. Cho et al. [13] demonstrated that a particular strain component, that is, the shear strain component, promotes grain subdivision under the same equivalent strain conditions in low-carbon steel. The strain state is hypothesized to influence mechanical properties via the deformed structures. However, the direct correlation between the strain components and mechanical properties has not been clarified.

Therefore, this study aimed to investigate the effects of wrought processes on the mechanical properties from the viewpoint of the strain components introduced by the processes. Different strain states with the same equivalent strain, 1.5, were induced by five wrought processes (forging, rolling, extrusion, equal-channel-angular-extrusion (ECAE), and caliber rolling) at 573 K. Combining the strain state computed by FEM and the mechanical properties examined by the ambient tensile test, the dependency of the mechanical properties on the wrought process was discussed.

2. Experimental procedure

Extruded Mg alloy AZ31 (Mg-3.0 Al-0.8 Zn-0.31 Mn, wt. %) was first annealed at 673 K for 1 h to remove the residual strain and then processed through five wrought processes (forging, rolling, extrusion, ECAE, and caliber rolling) at 573 K. The processing conditions were designed to induce an equivalent strain of 1.5 [6,14]. Details of the processing conditions have been reported elsewhere [9].

The mechanical properties were investigated by ambient tensile testing at a constant crosshead speed, corresponding to an initial strain rate of 1.0×10^{-3} s^{-1}. The tensile specimens were machined to have a gauge section that was 3 mm long, 1 mm wide, and 1 mm thick. The tensile directions were parallel to the transverse direction (TD) to compression direction (CD) in the forged alloy, the rolling direction (RD) in the rolled and caliber rolled alloys, and the extrusion direction (ED) in the extruded and ECAE alloys.

The strain states induced by the wrought processes were computed using FEM analysis [9]. The calculation results were analyzed in the orthogonal coordinate system, and the orientations of the x- and z-axes were parallel to (TD, CD) in forging, (RD, ND) in rolling and caliber

* Corresponding author.
** Corresponding author.
E-mail addresses: cyjk1504@mail4.doshisha.ac.jp, hyoshizumi3141@gmail.com (H. Yoshizumi), myuasa@mail.doshisha.ac.jp (M. Yuasa).

https://doi.org/10.1016/j.jmrt.2026.07.138
Received 21 May 2026; Received in revised form 7 July 2026; Accepted 17 July 2026
Available online 21 July 2026
2238-7854/

rolling, and (ED, ND) in extrusion and ECAE.

3. Results

The microstructures were observed using electron backscatter diffraction (EBSD) scanning electron microscopy (SEM). The EBSD observation results are shown in Supplementary Fig. S1. The EBSD results show that the basal texture developed clearly perpendicular to the compression direction (CD) in the forged alloy and parallel to the rolling direction (RD) in the rolled alloy (Fig. S1 (a) and (d)). The weak fiber basal texture evolved parallel to the extrusion direction (ED) in the extrusion and ECAE processes, and parallel to the RD in caliber rolling. To evaluate the intensity of this texture, X-ray diffraction (XRD) was performed along the CD in the forged alloy, normal direction (ND) to RD in the rolled alloy and caliber rolled alloy, and the ND to ED in the extruded alloy and ECAE-processed alloy. The basal plane orientation index I(basal)/I(total) was calculated from the XRD peak data to express the intensity of the basal texture [15].

The grain sizes and basal texture intensities are listed in Table 1. The detailed results of the microstructure observation have been reported [9]. The average grain size and grain size deviation were the largest for the forged alloy (Table 1). The forged alloy has a heterogeneous microstructure, which is a mixture of fine grains of several micrometers and coarse grains of approximately 70 μm (Fig. S1 (c)). The other alloys exhibited homogeneous microstructures composed of nearly average grain sizes (Fig. S1 (f)). The EBSD observation and XRD analysis showed that the basal texture developed far more intensively during forging and rolling (Fig. S1 (a) and (d)). The FEM results are listed in Table 2. These calculation results indicate that the processes introduced different strain states with comparable equivalent strain (1.65-1.90). All processes induce compressive strain along the z-axis, ε_{zz}, whose direction is parallel to the basal pole distributing concentratively. Further, the intensity of the basal texture increases with the compressive strain ε_{zz}. The authors previously reported a detailed discussion regarding the relationship between the strain state and microstructural evolution [9].

Fig. 1 shows the nominal stress–nominal strain curves, and Table 3 summarizes the tensile test results. To evaluate the dependence of the mechanical properties on the wrought process, the yield stress and uniform elongation are shown as functions of the compressive strain in the z-axis ε_{zz} in Fig. 2. With a larger induced compressive strain ε_{zz}, the yield stress increases, and conversely the uniform elongation decreases. However, the forged alloy, which induces the largest compressive strain ε_{zz}, does not follow these trends. It should be noted that the FEM analysis revealed a certain variation in the equivalent strain among the different wrought processes (Table 2). Although this variation may have contributed to the observed differences in microstructure and mechanical properties, it does not appear to fully explain the present results. For example, the forged alloy, despite exhibiting high equivalent strain, showed a mixture of fine and coarse grains. Whereas, the caliber rolled alloy, which exhibits relatively smaller equivalent strain, showed a homogeneous and fine-grained microstructure (Table 1). Therefore, these observations suggest that, within the range of equivalent strain variation examined in this study, the deformation path also plays an important role in determining the microstructure formation and mechanical properties. In the following sections, the relationships between the wrought process and mechanical properties are discussed based on the strengthening mechanism.

Table 1
Results of microstructure and texture observation.

	Forging	rolling	extrusion	ECAE	caliber rolling
grain size [μm]	20.9 ± 18.4	12.6 ± 5.8	12.2 ± 6.6	15.7 ± 10.4	7.7 ± 0.9
Intensity of basal texture *I*(*basal*)/*I*(*total*)	9.3	10.5	2.8	2.5	4.0

Table 2
Induced strain calculated by FEM analysis.

	Forging	rolling	extrusion	ECAE	caliber rolling
equivalent strain	1.87	1.90	1.67	1.68	1.65
ε_{zz}	−1.87	−1.44	−0.73	−0.26	−0.47

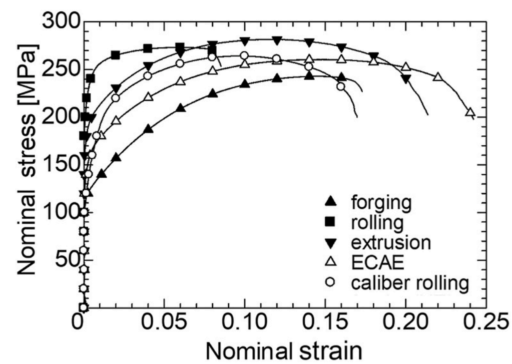

Fig. 1. Nominal stress–nominal strain curves obtained by ambient tensile test of wrought processed alloys.

Table 3
Mechanical properties in the tensile test.

	yield stress [MPa]	ultimate tension stress [MPa]	uniform elongation [%]	fracture elongation [%]
forging	132.1 ± 15.0	239.9 ± 7.6	13.0 ± 1.2	17.1 ± 0.8
rolling	227.6 ± 5.4	283.3 ± 7.7	6.4 ± 0.4	9.6 ± 1.2
extrusion	171.3 ± 10.7	279.7 ± 3.3	12.1 ± 0.5	21.4 ± 0.8
ECAE	150.9 ± 8.4	259.1 ± 3.4	14.9 ± 0.4	23.5 ± 0.8
caliber rolling	174.5 ± 2.5	266.6 ± 2.6	9.1 ± 0.2	17.3 ± 1.0

4. Discussion

4.1. Effect of the wrought process on the yield stress

Supplementary Fig. S2 shows the effects of the grain size and basal texture on the yield stress. The yield stress was strengthened by grain size refinement according to the Hall–Petch relationship (Fig. S2 (a)). Although the rolled and extruded alloys have similar grain sizes, the yield stress of the rolled alloy was approximately 50 MPa higher than that of the extruded alloys. This difference was due to the basal texture intensity (Fig. S2 (b)). However, the forged alloy with strong basal texture was barely strengthened. To distinguish the strengthening mechanism in the forged alloy, the contributions of grain size, basal texture, and work hardening by the processes were assessed by referring to Refs. [16,17] (Supplementary B), and the results are summarized in Fig. 3. Fig. 3 shows that the rolled alloy was strengthened by grain size refinement and texture evolution. The alloys that have smaller compressive strain ε_{zz} (extrusion, ECAE, and caliber rolling) were strengthened only by grain size refinement and softened by the effect of texture. These expected yield stresses are close to the experimentally measured values. Nevertheless, the yield stress of the forged alloy was overestimated by 40 MPa, which is higher than the experimentally measured value. The experimentally measured value is in good agreement with the sum of the yield stress of the non-processed alloy (HT) and the contribution of the grain size, which is consistent with the lower strengthening of the forged alloy by the basal texture in Fig. S2(b).

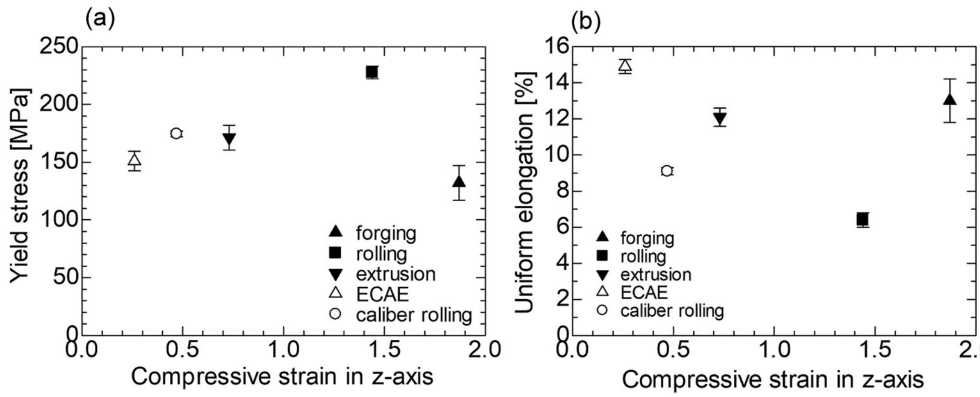

Fig. 2. Effects of the compressive strain induced in wrought processes along the z-axis on the mechanical properties: (a) yield stress, (b) uniform elongation.

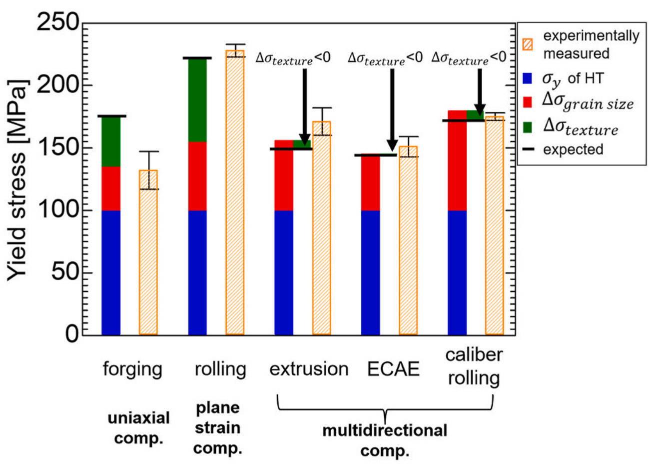

Fig. 3. Comparison of the experimentally measured yield stress with the expected yield stress based on assessments of strengthening by grain size refinement and basal texture development.

When tensile tests were conducted on the TD of the forged alloy, the tensile direction was parallel to the basal texture (Fig. S1 (a)). Under these conditions, the Schmid factor of basal slip was low (Table S1). As a result, it is difficult for basal slip to occur, and the yield stress is expected to increase. However, the forged alloy has a mixture of coarse and fine grains, and the yield stress cannot be discussed only in terms of texture. Cepeda-Jiménez et al. [18] reported that grain size refinement decreased the activity of non-basal slip and restricted the deformation mechanism to basal slip, even in an intensive basal texture. Schmid factor distributions are shown in Supplementary Fig. S3. The coarse grains exhibit relatively low Schmid factors for basal slip, whereas higher Schmid factors are observed for the non-basal slip systems. These results indicate that deformation in the coarse grains can be accommodated by non-basal slip in addition to basal slip. Because the non-basal slip can achieve a high magnitude of strain for the basal slip in coarse grains, the forged alloy lacks strengthening by the basal texture.

Fig. 2 (a) shows that the wrought process inducing a larger compressive strain ε_{zz} strengthens yield stress. Using the compressive strain ε_{zz}, the strain states applied by the five wrought processes can be classified quantitatively [9]. When the equivalent strain $\bar{\varepsilon}$ is applied, the compressive strain ε_{zz} of the forged, rolled, and the other processed alloys are $|\varepsilon_{zz}| = \bar{\varepsilon}, \sqrt{3}\bar{\varepsilon}/2$, and $< \bar{\varepsilon}/2$. These strain states correspond to uniaxial compression, plane strain compression, and multidirectional compression, respectively. From the viewpoint of the strain state, the correlation between the compressive strain ε_{zz} and the microstructure evolution can be expressed as follows: the basal texture becomes more intensive, and the grain size becomes larger and inhomogeneous through the transition of the strain state from multidirectional compression to uniaxial compression (Tables 1 and 2). Thus, Fig. 2 (a) shows that the transition from multidirectional compression to plane strain compression intensifies the basal texture and consequently increases the yield stress. When the strain state is uniaxial compression, the uniaxially compressed alloy is not strengthened by the basal texture because the microstructure becomes a mixture of coarse and fine grains.

4.2. Effects of wrought processes on uniform elongation

Previous studies have reported that grain size refinement enhances ductility by inhibiting twin activity [19,20]. The $\{10\bar{1}2\}$ tensile twin operates easily next to the basal slip to achieve a tensile strain along the c-axis under ambient deformation. The stress–strain curve of the twin-dominant deformation is characterized by a concave curve [21]. However, no concave curves are observed in Fig. 1, indicating that the twin activity does not dominate the tensile deformation in any of the processed alloys. The low activity of the twin is ascribed to the orientation relationship between the basal texture and the tensile direction. In the forged and rolled alloys, the tensile direction was parallel to the basal texture, and it was difficult for the twin to act. In other alloys, tensile deformation can be achieved by basal slip without the twin because the basal texture is weak. Therefore, the dependence of the uniform elongation on the wrought process cannot be rationalized by twin activity.

Unlike the grain size, the basal texture is significantly related to the uniform elongation in Fig. 4. An increase in the intensity of the basal texture decreases the uniform elongation, except for the forged alloy. Because the twin hardly acts, the relationship between the uniform elongation and basal texture is rationalized by the difference in slip activity. Valle et al. [22] reported that dynamic recovery was activated by a non-basal slip system in an alloy with an intensive basal texture. To

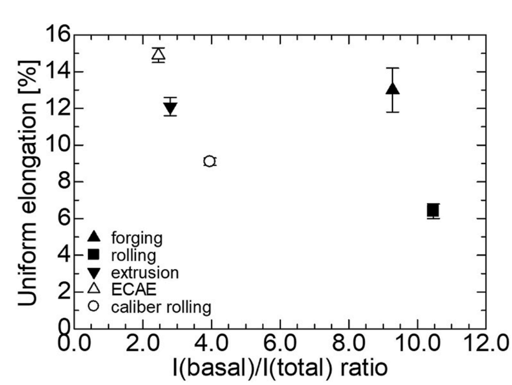

Fig. 4. Relationship between uniform elongation and intensity of the basal texture.

assess the dynamic recovery due to the difference in slip activity, Fig. 5 (a) shows the work-hardening behavior after the yield stress. In all alloys, the work-hardening rate decreased linearly, indicating stage III work hardening. In this stage, the dynamic recovery annihilates the stored dislocations and decreases the work-hardening rate. Stage III was modeled using the following equation [22]:

$$\theta = \frac{d\sigma}{d\varepsilon} = \theta_0\left(1 - \frac{\sigma - \sigma_y}{\sigma_s}\right), \tag{1}$$

where θ_0 is the work-hardening rate at the yield stress, σ_y is the yield stress, and the σ_s is the saturated stress. Kocks & Mecking [23] proposed the evolution model of the dislocation density ρ in stage III as follows:

$$\frac{d\rho}{d\varepsilon} = k_1\sqrt{\rho} - k_2\rho \tag{2}$$

Here, $k_1\sqrt{\rho}$ is a term associated with the rate of accumulation of dislocations and $-k_2\rho$ is related to the annihilation of the dislocations by the dynamic recovery. The flow stress is expressed as follows:

$$\sigma = \sigma_y + M\alpha Gb\sqrt{\rho} \tag{3}$$

where M is the Taylor factor, α is a constant, G is the shear module, and b denotes the Burgers vector [22]. Using Eqs. (2) and (3), the work-hardening rate can be described as follows:

$$\theta = \frac{M\alpha Gb}{2}k_1 - \frac{k_2}{2}(\sigma - \sigma_y) \tag{4}$$

Comparing Eqs. (1) and (4), the factor governing the rate of dynamic recovery k_2 can be written as

$$k_2 = \frac{2\theta_0}{\sigma_s} \tag{5}$$

The slope of stage III (θ_0/σ_s) can quantify the activity of the dynamic recovery. Fig. 5(b) shows the influence of dynamic recovery on the uniform elongation. The uniform elongation decreased with an increase in the magnitude of the slope of stage III, which agrees with previous studies [24–26]. The dynamic recovery annihilates the stored dislocations and degrades the work hardenability, decreasing the uniform elongation. This tendency is generally consistent with the relationship shown in Fig. 4, where alloys with stronger basal texture tend to exhibit lower uniform elongation.

Although the forged alloy had an intense basal texture, its uniform elongation was close to that of alloys with a weak basal texture, as shown in Fig. 4. This is because of the heterogeneous microstructure composed of coarse and fine grains. Several studies reported that the Mg alloy with heterogeneous microstructure exhibits good ductility [27–29]. According to Wei et al. [29], the deformation incompatibility at the grain boundaries between coarse and fine grains causes geometrically necessary dislocations (GNDs). Supplementary Fig. S4 shows the IPF maps and grain reference orientation deviation (GROD) maps of tensile samples. In the tensile sample from forged alloy, the high GROD values are observed in vicinity of the boundaries of coarse sized grains, indicated by white arrows in Supplementary Fig. S4 (b). Additionally, the high GROD regions are rarely observed in fine sized grains. In the tensile sample from rolled alloy, although the high values of GROD are observed, these distributions are not related to the grain size (Fig. S4 (d)). Thus, GNDs were frequently induced in the forged alloy with heterogeneous grain sized microstructure. These GNDs impede dislocation gliding and cause work hardening, consequently enhancing ductility. The heterogeneous microstructure of the forged alloy was the reason for its good ductility despite its intensive basal texture.

Fig. 2(b) shows that the increase in compressive strain ε_{zz} induced by the wrought processes degrades the ductility. However, under uniaxial compression, the microstructure composed of coarse and fine grains improved the work hardenability, and the ductility was enhanced, even with an intensive texture.

5. Conclusions

The AZ31 Mg alloy was subjected to an equivalent strain of approximately 1.5 via five wrought processes (forging, rolling, extrusion, ECAE, and caliber rolling) at 573 K. The strain state induced by these processes was computed using FEM. The mechanical properties of the processed alloys were examined using ambient tensile tests. These results led to the following conclusions.

(1) The yield stress increased with increasing compressive strain applied during these processes. The larger the induced compressive strain, the more intensive was the development of the basal texture, and this texture increased the yield stress. However, the forged alloy, which had the largest compressive strain, was not strengthened by texture intensification owing to its heterogeneous microstructure composed of fine and coarse grains.

(2) Uniform elongation decreased with increasing compressive strain applied during the processes. The basal texture intensified by the large compressive strain promoted dynamic recovery, consequently degrading work hardenability and uniform elongation. However, in the forged alloy, the deformation incompatibility between the fine and coarse grains enhanced the work hardenability, resulting in a highly uniform elongation despite the sharp basal texture.

CRediT authorship contribution statement

Hiromasa Yoshizumi: Writing – original draft, Validation,

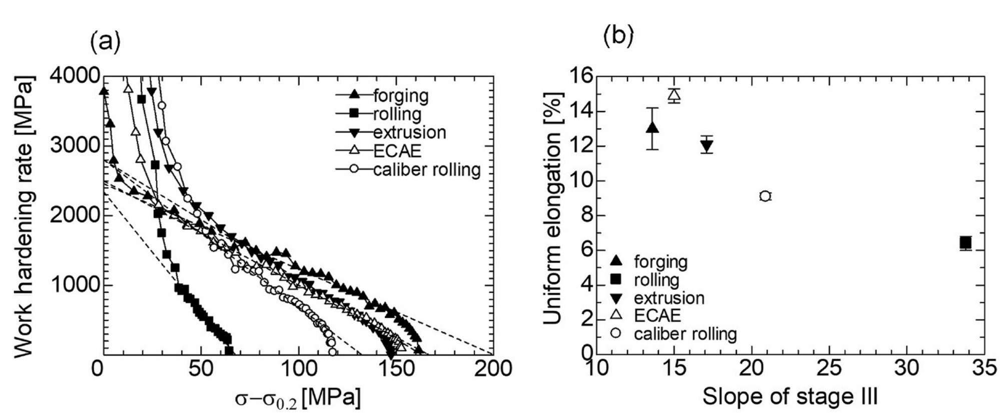

Fig. 5. (a) Work hardening rate illustrated as functions of $\sigma - \sigma_y$ and (b) relationship between uniform elongation and the slope of work hardening stage III in (a), which corresponds to the activity of the dynamic recovery.

Investigation, Data curation, Conceptualization. Motohiro Yuasa: Writing –review & editing, Validation, Investigation, Supervision, Conceptualization, Project administration. Hiroyuki Miyamoto: Writing – review & editing, Validation, Supervision. Hidetoshi Somekawa: Writing– review & editing, Validation, Conceptualization.

Declaration of competing interest

The authors declare that they have no known competing financial interests or personal relationships that could have appeared to influence the work reported in this paper.

Acknowledgement

This work was supported by JST SPRING, Grant Number JPMJSP2129.

Appendix A. Supplementary data

Supplementary data to this article can be found online at https://doi.org/10.1016/j.jmrt.2026.07.138.

References

[1] Ebrahimi M, Wang Q, Attarilar S. A comprehensive review of magnesium-based alloys and composites processed by cyclic extrusion compression and the related techniques. Prog Mater Sci 2023;131:101016. https://doi.org/10.1016/j.pmatsci.2022.101016.
[2] Tripathi A, Murty SVSN, Narayanan PR. Microstructure and texture evolution in AZ31 magnesium alloy during caliber rolling at different temperatures. J Magnesium Alloys 2017;5:340–7. https://doi.org/10.1016/j.jma.2017.07.001.
[3] Sabat RK, Brahme AP, Mishra RK, Inal K, Suwas S. Ductility enhancement in Mg-0.2%Ce alloys. Acta Mater 2018;161:246–57. https://doi.org/10.1016/j.actamat.2018.09.023.
[4] Cui C, Zhang W, Chen W, He J, Chen X, Hou J. Microstructure, texture evolution and yield strength symmetry improvement of as-extruded ZK60 Mg alloy via multi-directional impact forging. J Magnesium Alloys 2022;10:2745–60. https://doi.org/10.1016/j.jma.2021.01.001.
[5] Mukai T, Somekawa H, Inoue T, Singh A. Strengthening Mg-Al-Zn alloy by repetitive oblique shear strain with caliber roll. Scr Mater 2010;62:113–6. https://doi.org/10.1016/j.scriptamat.2009.09.005.
[6] Inoue T, Somekawa H, Mukai T. Hardness variation and strain distribution in magnesium alloy AZ31 processed by multi-pass caliber rolling. Adv Eng Mater 2009;11:654–8. https://doi.org/10.1002/adem.200900103.
[7] Inoue T, Horita Z, Somekawa H, Ogawa K. Effect of initial grain sizes on hardness variation and strain distribution of pure aluminum severely deformed by compression tests. Acta Mater 2008;56:6291–303. https://doi.org/10.1016/j.actamat.2008.08.042.
[8] Suwas S, Gottstein G, Kumar R. Evolution of crystallographic texture during equal channel angular extrusion (ECAE) and its effects on secondary processing of magnesium. Mater Sci Eng, A 2007;471:1–14. https://doi.org/10.1016/j.msea.2007.05.030.
[9] Yoshizumi H, Yuasa M, Miyamoto H, Somekawa H. Influence of different wrought processes on the microstructure and texture evolution in AZ31 magnesium alloy. Mater Charact 2024;217:114446. https://doi.org/10.1016/j.matchar.2024.114446.
[10] Kang J-H, Inoue T, Torizuka S. Effect of shear strain on the microstructural evolution of a low carbon steel during warm deformation. Mater Trans 2010;51:27–35. https://doi.org/10.2320/matertrans.MB200916.
[11] Inoue T, Ueji R. Effect of strain and deformation mode on cube texture formation in warm bi-axial rolled low-carbon steel. Finite Elem Anal Des 2021;183–184:103491. https://doi.org/10.1016/j.finel.2020.103491.
[12] Kamikawa N, Sakai T, Tsuji N. Effect of redundant shear strain on microstructure and texture evolution during accumulative roll-bonding in ultralow carbon IF steel. Acta Mater 2007;55:5873–88. https://doi.org/10.1016/j.actamat.2007.07.002.
[13] Cho J-Y, Inoue T, Yin F, Nagai K. Effect of shear deformation on microstructural evolution of Ni-30Fe alloy during hot deformation. Mater Trans 2004;45:2966–73. https://doi.org/10.2320/matertrans.45.2966.
[14] Iwahashi Y, Wang J, Horita Z, Nemoto M. Principle of equal-channel angular pressing for the processing of ultra-fine grained materials. Scripta Metall Mater 1996;35:143–6.
[15] Robin A, Martinez GAS, Suzuki PA. Effect of cold-working process on corrosion behavior of copper. Mater Des 2012;34:319–24. https://doi.org/10.1016/j.matdes.2011.08.018.
[16] Hagihara K, Li Z, Yamasaki M, Kawamura Y, Nakano T. Strengthening mechanisms acting in extruded Mg-based long-period stacking ordered (LPSO)-Phase alloys. Acta Mater 2019;163:226–39. https://doi.org/10.1016/j.actamat.2018.10.016.
[17] Wei K, Hu R, Yin D, Xiao L, Pang S, Cao Y, et al. Grain size effect on tensile properties and slip systems of pure magnesium. Acta Mater 2021;206:116604. https://doi.org/10.1016/j.actamat.2020.116604.
[18] Cepeda-Jiménez CM, Molina-Aldareguia JM, Pérez-Prado MT. Effect of grain size on slip activity in pure magnesium polycrystals. Acta Mater 2015;84:443–56. https://doi.org/10.1016/j.actamat.2014.10.001.
[19] Barnett MR, Keshavarz Z, Beer AG, Atwell D. Influence of grain size on the compressive deformation of wrought Mg-3Al-1Zn. Acta Mater 2004;52:5093–103. https://doi.org/10.1016/j.actamat.2004.07.015.
[20] Somekawa H, Nakajima K, Singh A, Mukai T. Ductile fracture mechanism in fine-grained magnesium alloy. Philos Mag Lett 2010;90:831–9. https://doi.org/10.1080/09500839.2010.508444.
[21] Hong S-G, Park SH, Lee CS. Role of {10-12} twinning characteristics in the deformation behavior of a polycrystalline magnesium alloy. Acta Mater 2010;58:5873–85. https://doi.org/10.1016/j.actamat.2010.07.002.
[22] Del Valle JA, Carreño F, Ruano OA. Influence of texture and grain size on work hardening and ductility in magnesium-based alloys processed by ECAP and rolling. Acta Mater 2006;54:4247–59. https://doi.org/10.1016/j.actamat.2006.05.018.
[23] Kocks UF, Mecking H. Physics and phenomenology of strain hardening: the FCC case. Prog Mater Sci 2003;48:171–273. https://doi.org/10.1016/S0079-6425(02)00003-8.
[24] Huang X, Suzuki K, Watazu A, Shigematsu I, Saito N. Mechanical properties of Mg-Al-Zn alloy with a tilted basal texture obtained by differential speed rolling. Mater Sci Eng, A 2008;488:214–20. https://doi.org/10.1016/j.msea.2007.11.029.
[25] Yuan W, Mishra RS. Grain size and texture effects on deformation behavior of AZ31 magnesium alloy. Mater Sci Eng, A 2012;558:716–24. https://doi.org/10.1016/j.msea.2012.08.080.
[26] Kumar N, Dendge N, Banerjee R, Mishra RS. Effect of microstructure on the uniaxial tensile deformation behavior of Mg-4Y-3RE alloy. Mater Sci Eng, A 2014;590:116–31. https://doi.org/10.1016/j.msea.2013.10.009.
[27] Li JR, Zeng ZR, Song B, Xie HB, Pei RS, Pan HC, et al. Mechanical investigation on Ce addition in tuning recrystallization behavior and mechanical property of Mg alloy. J Mater Sci Technol 2023;132:1–17.
[28] Wang Y, Choo H. Influence of texture on hall-petch relationships in an Mg alloy. Acta Mater 2014;81:83–97. https://doi.org/10.1016/j.actamat.2014.08.023.
[29] Wei X, Jin L, Wang F, Li J, Ye N, Zhang Z, et al. High strength and ductility Mg-8Gd-3Y-0.5Zr alloy with bimodal structure and nano-precipitates. J Mater Sci Technol 2020;44:19–23. https://doi.org/10.1016/j.jmst.2019.10.024.